

Thiazolyl-linked conjugated microporous polymers for enhancement adsorption and photocatalytic degradation of organic dyes from water



A.F. Saber ^a, C.-C. Chueh ^{b, c}, M. Rashad ^{d, e}, S.-W. Kuo ^{a, **}, A.F.M. EL-Mahdy ^{a, f, *}

^a Department of Materials and Optoelectronic Science, National Sun Yat-Sen University, Kaohsiung 80424, Taiwan

^b Department of Chemical Engineering, National Taiwan University, Taipei 10617, Taiwan

^c Advanced Research Center for Green Materials Science and Technology, National Taiwan University, Taipei 10617, Taiwan

^d Physics Department, Faculty of Science, University of Tabuk, Tabuk 71491, Saudi Arabia

^e Physics Department, Faculty of Science, Assiut University, Assiut 71516, Egypt

^f Chemistry Department, Faculty of Science, Assiut University, Assiut 71516, Egypt

ARTICLE INFO

Article history:

Received 14 February 2023

Received in revised form

3 May 2023

Accepted 3 June 2023

Available online 7 June 2023

Keywords:

Conjugated microporous polymers

thiazolyl[5,4-d]thiazole

Dye uptake

Rhodamine B

Methylene blue

Photocatalysis

ABSTRACT

Organic dyes and pigments are common examples of pollutants that have been drained to water resources. Subsequently, chemists searched for novel and efficient adsorbents for treatment of sewage water from coloring compounds. Conjugated microporous polymers (CMPs), which displayed high Brunauer Emmett and Teller (BET) surface area and porous morphology, beside other unique merits, solve this challenging situation by consuming dye molecules into their large and permanent pores, and degrading them in the presence of light. In this paper, we adopt a designed synthesis of new thiazolyl-linked CMPs containing bicarbazole, bifluorenylidene, and biphenylethene building blocks, namely: BC-TT, BF-TT, and BIPE-TT CMPs, respectively. All the common characterizations including chemical, physical, and photophysical were conducted for the as-synthesized CMPs. In addition to their significant surface areas that reach 522 m²/g and maximum pore volumes (up to 0.50 cm³/g), they possessed good thermal stabilities with the highest values (degradation temperature = 460 °C; char yield = 67 wt%). Furthermore, the produced polymers have been proven to have adsorption capability as well as photocatalytic degradation for both Rhodamine B (RhB) and methylene blue (MB) dyes. BC-TT CMP exhibited the highest adsorption efficiency among others toward the RhB dye with a capacity of 228.83 mg/g, as well as the maximum performance for MB dye uptake (up to 232.02 mg/g). After measuring the photocatalytic degradation of dyes using these CMPs, BC-TT-CMP also showed the top value of catalytic efficiency at all, either for RhB (rate constant: 2.5 × 10⁻² min⁻¹) or MB dye (rate constant: 3.5 × 10⁻² min⁻¹).

© 2023 Elsevier Ltd. All rights reserved.

1. Introduction

For the time being, chemical dyes and tinctures are vastly applied by numerous industries (such as texture, leather, pharmaceutical, cosmetic, and nutrition industries), and they are mainly considered as one of water pollutants regarding their toxicity, chemical stability, and difficulty of degradation [1,2]. Each year, large quantities of coloring materials exceeding 7 × 10⁵ tons in weight are utilized worldwide, about 10–15% of which are drained as effluents into water sources, threatening human health as well as

many living organisms, fishing, and other life activities [3], due to their carcinogenic, mutagenic, teratogenic, and toxic effects [4–7]. For example, many ailments including vomiting, diarrhea, and inflammation were caused because of methylene blue (MB) dye consumption; in addition, the level of inverse influence of MB in rats was recorded as 50 mg/kg and greater [8]. Consequently, various mechanisms either physical, chemical, or biological have been improved for dyes elimination such as catalysis, adsorption, sedimentation, membrane filtration, ion exchange, coagulation, and biodegradation [9–12]. The adsorption technique is among the most applied methods for sewage treatment [13,14]. Recently, a new type of adsorbent materials called porous organic polymers (POPs) have attracted attention, owing to their depressed skeletal density, surface area elevation, synthetic routes flexibility, simple functionalization, good thermal and physicochemical stability, and

* Corresponding author.

** Corresponding author.

E-mail addresses: kuosw@faculty.nsysu.edu.tw (S.-W. Kuo), ahmedelmahdy@mail.nsysu.edu.tw (A.F.M. EL-Mahdy).

decreased cost [15–22]. Moreover, introducing specific functional groups such as amino ($-\text{NH}_2$) [23], hydroxyl ($-\text{OH}$) [24], sulfonic acid ($-\text{SO}_3\text{H}$) [25], and carboxyl ($-\text{COOH}$) groups [26] into POPs has been utilized specially in dye adsorption. Diverse types of POPs have been reported and studied as porous aromatic frameworks (PAFs) [27], conjugated microporous polymers (CMPs) [28–31], covalent organic frameworks (COFs) [32–35], and others [36,37].

CMPs are a promising subcategorized kind of POPs that reign lots of qualities over other POPs, such as large specific surface areas, excellent stability, and good photophysical properties, in addition to various applications ranging from those concerning to sustainable energy, such as batteries [38–40], thermoelectrics [41], sensors [42,43], transistors [44–48], supercapacitors [49–51], and light emitting diodes [52–55], to gas adsorption and separation [56], hydrophobic separation [57,58], light harvesting [59,60], and antibacterial applications [61]. Nowadays, photocatalysis is utilized side by side with the physisorption technique in solving environmental issues [62,63] to overcome some drawbacks of incomplete degradation and restoration of conventional porous materials. Photodegradation became one of the most recently used strategies for removal of organic dyes from aqueous solutions [64]. Thiazolo [5,4-*d*]thiazole is an important building block that has been used in many applications due to its rigidity and aromaticity. Some derivatives containing this core such as 2,5-bis(4-pyridyl)thiazolo [5,4-*d*]thiazole were reported to possess high fluorescence properties [65]. Furthermore, fused thiazolo[5,4-*d*]thiazoles have attracted other applications in organic semiconductors [66–69] and optoelectronics [70,71]. In addition, CMPs linked by thiazolyl [5,4-*d*]thiazole bridge have been used as adsorbents for CO_2 gas with a high selectivity [72] and in organic solar cells [73] and photocatalysis [74].

In the presented work, we displayed the synthesis of new conjugated CMPs that were connected together with the thiazolyl[5,4-*d*]thiazole knit, via the condensation reaction of dithiooxamide (TT) with 4,4',4''-(9,9'-bicarbazole)-3,3',6,6'-tetrayl) tetrabenzaldehyde (BC-4CHO, Schemes S1 and S2); 4,4',4''-(9,9'-bifluorenylidene)-3,3',6,6'-tetrayl) tetrabenzaldehyde (BF-4CHO, Schemes S3 and S4); and (*E*)-5',5'''-(ethene-1,2-diyl)bis([1'',1''':3''',1''''-terphenyl]-4,4''-dicarbaldehyde) (BIPE-4CHO, Schemes S5 and S6) to afford BC-TT, BF-TT, and BIPE-TT CMPs, respectively, using dimethyl formamide (DMF) as a solvent [Scheme 1 and S7–S9]. Many techniques have been utilized to emphasize and characterize the physiochemical, photophysical, and morphological properties of the produced thiazolyl-linked polymers including Fourier transform infrared (FTIR) spectroscopy, ultraviolet (UV)-Visible spectroscopy, photoluminescence (PL), solid-state ^{13}C nuclear magnetic resonance (NMR), thermogravimetric analysis (TGA), Brunauer Emmett and Teller (BET), scanning electron microscopy (SEM), and transmission electron microscopy (TEM). The reaction yield was very good; also, the thermal stabilities measurements were recorded with good performance. They have significant surface areas that have been investigated before carrying out organic dye adsorption and degradation. It is the first time to prepare and utilize thiazolyl-linked CMPs in photodegradation application of dyes, and the obtained data revealed that they have an excellent ability of both conventional physisorption and photodegradation of Rhodamine B (RhB) and MB organic dyes in aqueous solutions.

2. Material and methods

2.1. Materials

All solvents and chemicals were obtained from commercial suppliers and used as received unless otherwise noted. Carbazole (>95%), N-bromosuccinimide (>99%), potassium permanganate

(>99.0%), 4-formylphenylboronic acid (95%), 3,5-dibromobenzaldehyde, dithiooxamide, potassium hydroxide, bromine, nitrobenzene, titanium tetrachloride, zinc metal, and sulfuric acid were ordered from Sigma-Aldrich. Tetrakis(triphenylphosphine)palladium(0) (99%), was purchased from Acros, whereas phenanthrene-9,10-dione and Lawesson's reagent were ordered from Alfa Aesar. Ethanol was gained from Kelong Chemistry Reagent Co. Ltd. (Chengdu, China).

2.2. Synthesis of (*E*)-5',5'''-(ethene-1,2-diyl)bis([1'',1''':3''',1''''-terphenyl]-4,4''-dicarbaldehyde) (BIPE-4CHO)

BIPE-4Br (0.76 g, 1.54 mmol), 4-formylphenylboronic acid (1.85 g, 12.3 mmol), $\text{Pd}(\text{PPh}_3)_4$ (90.0 mg, 0.0780 mmol), and K_2CO_3 (2.13 g, 15.4 mmol) were added in a two-neck flask and subjected to vacuum for 15 min. Dioxane (50 mL) and H_2O (8 mL) were added and then the mixture was heated at 100°C for 48 h. The solution was poured into a stirred beaker filled with ice cubes and H_2O . The solid was separated using a suction filter, placed in a beaker, and treated with a little MeOH; the mixture was heated until it boiled, and then the solution was sonicated for 15 min. The undissolved solid was separated using a suction filter, placed in a beaker, and treated with a small amount of dichloromethane (DCM); heated until it boiled, followed by sonication for 15 min. After suction filtering, the undissolved solid was dried in an oven for 24 h to obtain a gray solid (Yield, 79%).

2.3. General synthesis of BC-TT, BF-TT, and BIPE-TT CMPs

In a 25-mL Pyrex tube, a mixture of BC-4CHO, BF-4CHO, and BIPE-4CHO (0.13 mmol) and TT (0.27 mmol) were evacuated for 15 min. Then, DMF (5 mL) was added and sonicated for 2 min. Degassing of the mixture by three freeze–pump–thaw cycles and purging with N_2 was carried out to remove the oxygen from the system. The tube was then heated at 140°C for 48 h. After cooling to room temperature (25°C), the reaction mixture was centrifuged and washed 3 times with DMF and three times with tetrahydrofuran (THF) till a colorless solution was obtained. Finally, the obtained precipitate was dried at 100°C overnight under vacuum to yield CMPs.

2.4. Photodegradation experiments

To exclude the decomposition of RhB and MB upon UV irradiation, a >450-nm optical filter was set in front of the xenon lamp light source (300 W) to cut off UV light and make sure that photocatalytic degradation is induced by visible light. The distance between the liquid level and the filter is fixed at 6 cm. In a typical photodegradation experiment, 7 mg of thiazolyl-linked CMPs (BC-TT CMP, BF-TT CMP, BIPE-TT CMP) was added to 56 mL of RhB dye–aqueous solution (20 mg/L for BC-TT CMP, 10 mg/L for both BF-TT and BIPE-TT CMPs) and magnetically stirred with the rate of 800 rpm for 60 min in the dark for reaching the saturation of adsorption of dye. After that, the mixture was illuminated with visible light for another 3 h in the air. The suspension was separated by centrifugation at different time intervals, and the centrifugation time of each separation was kept for 5 min at 12,000 rpm; then UV-visible spectra was recorded with 1 cm cuvettes.

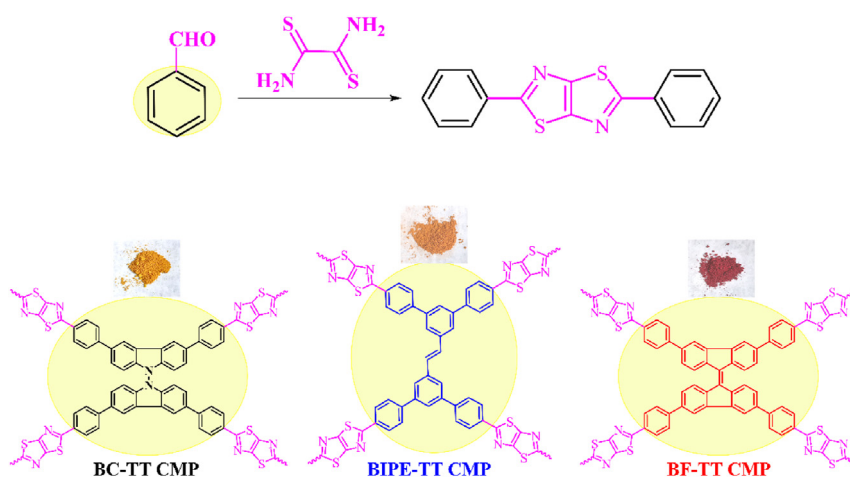
3. Results and discussions

3.1. CMPs synthesis and characterizations

The major goal of this work is to construct thiazolyl-linked CMPs containing bicarbazole, bifluorenylidene, and diphenylethene

structural units, as well as testing their performance toward dye removal and photocatalytic degradation. The first and second starting monomers 4,4',4'',4'''-([9,9'-bicarbazole]-3,3',6,6'-tetrayl)-tetrabenz aldehyde (BC-4CHO) and 4,4',4'',4'''-([9,9'-bifluorenylidene]-3,3',6,6'-tetrayl)-tetrabenz aldehyde (BF-4CHO), respectively, have been synthesized according to the recently reported literature of our group (Schemes S1–S4 and Figs. S1 and S2) [75,76]. The third building block (*E*)-5',5''''-(ethene-1,2-diyl)bis((1,1':3',1''-terphenyl)-4,4''-dicarbaldehyde) (BIPE-4CHO) was a new one that has been prepared by the reductive coupling of 3,5-dibromobenzaldehyde using Zn metal and TiCl₄ in THF to yield (*E*)-1,2-bis(3,5-dibromophenyl)ethene compound (BIPE-4Br) (Scheme S5), which further reacted via Pd-catalyzed Suzuki coupling with (4-formylphenyl)boronic acid in the presence of K₂CO₃ in dioxane, producing the final derivative (Scheme S6). Confirmation of the chemical structure of this novel monomer was carried out using FTIR and NMR spectroscopy. From FTIR spectroscopy, one can notice the disappearance of the absorption band

at 624 cm⁻¹ characteristic of C–Br bond and the apparition of other two absorption bands at 1,693 and 2,850 cm⁻¹, corresponding to C=O and C–H formyl stretching bonds, respectively (Fig. S3). In addition, ¹H NMR spectrum represented a sharp singlet signal at 10.12 ppm featured to the formyl protons, a singlet signal at 7.81 ppm for C=C, and multiplet signals at 8.09, 8.15 ppm attributed to the phenyl protons (ArH) as well (Fig. S4). Furthermore, ¹³C NMR spectrum of BIPE-4CHO had two signals centered at 126.11 and 193.85 ppm characteristics of C=C and formyl carbons, respectively (Fig. S5). The targeted BC-TT CMP, BF-TT CMP, and BIPE-TT CMP were obtained through the polymerization condensation of the presynthesized monomers: BC-4CHO, BF-4CHO, and BIPE-4CHO, respectively, with TT in the presence of DMF solvent, as shown in Scheme 1. The cross-linking degrees of these CMPs were physically confirmed by their difficulty of solubility in various organic solvents such as methanol, ethanol, acetone, dimethyl formamide, and tetrahydrofuran. The successful condensation of the monomers with TT to provide the corresponding CMPs was



Scheme 1. Synthetic scheme of the thiazolyl-linked conjugated microporous polymers.

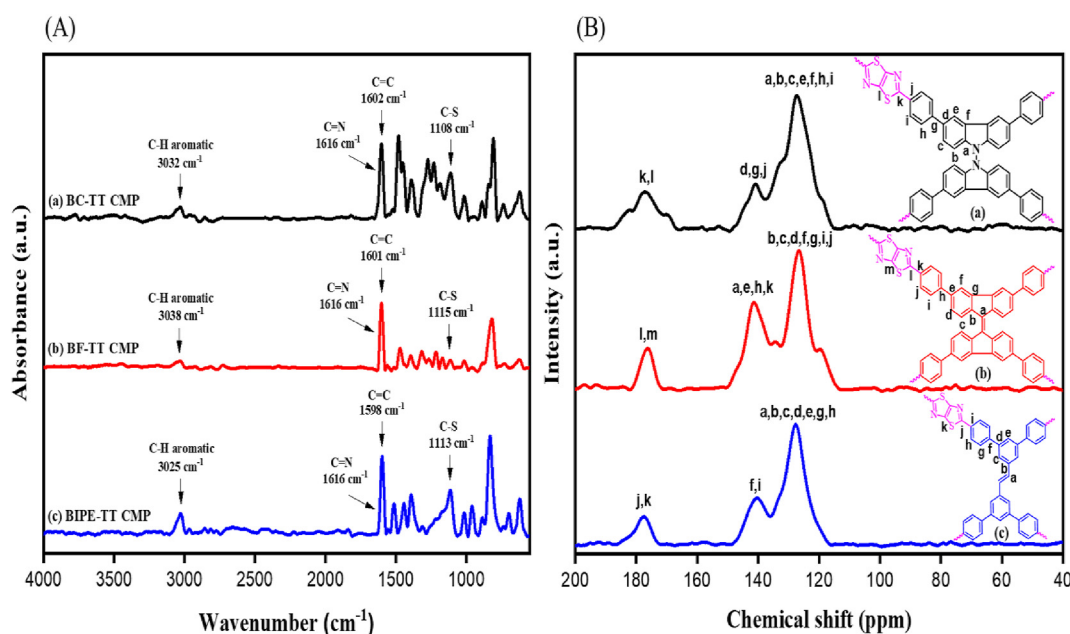


Fig. 1. (A) Fourier transform infrared spectra of the as-prepared (a) BC-TT, (b) BF-TT, and (c) BIPE-TT conjugated microporous polymers (CMPs). (B) ¹³C nuclear magnetic resonance spectroscopy of the produced (a) BC-TT, (b) BF-TT, and (c) BIPE-TT CMPs.

emphasized by the utilization of FTIR and ^{13}C -solid-state NMR techniques. Infrared spectra for all the three novel CMPs (Figs. S6–S8), BC-TT, BF-TT, and BIPE-TT, do not have the two vibrational peaks characteristic of the C=O and formyl hydrogen at 1,698 and 2,821 cm^{-1} , respectively, for BC-4CHO; at 1,693 and 2,858 cm^{-1} , respectively, for BF-4CHO; and at 1,693 and 2,850 cm^{-1} , respectively, for BIPE-4CHO. Also, there is a complete disappearance of absorption bands at 3,298, 3,211, 3,138, and 1,588 cm^{-1} attributed to NH_2 and C=S stretching vibrations, respectively, of the TT (Fig. 1A). On the other hand, new absorption bands corresponding to the thiazole C=N and C–S stretching vibrations were originated at 1,616 and 1,108 cm^{-1} , respectively, for BC-TT CMP; at 1,616 and 1,115 cm^{-1} , respectively, for BF-TT CMP; and at 1,616 and 1,113 cm^{-1} , respectively, for BIPE-TT CMP. Moreover, the solid-state ^{13}C NMR spectra represented ranged signals for the carbon nuclei of benzene rings at 147.11–116.04, 149.09–114.43, and 146.92–116.79 ppm for BC-TT, BF-TT, and BIPE-TT CMPs, respectively. Furthermore, additional signals existed at 177.22, 175.98, 177.48 ppm featuring C=N carbon for BC-TT, BF-TT, and BIPE-TT CMPs, respectively (Fig. 1B). Powder-X ray diffraction analysis of BC-TT, BF-TT, and BIPE-TT CMPs displayed no diffraction signals, indicating the amorphous aggregated nature of all the polymers (Fig. S9). TGA also confirms the complete chemical reaction between the monomers to yield thermally stable CMPs at higher temperatures. Measuring TGA under an N_2 atmosphere indicated that BC-TT CMP has the maximum value of thermostability that enabled it to be utilized in practical applications at elevated temperatures, with a degradation temperature (T_{d10}) and char yield values of 460 $^\circ\text{C}$ and 67 wt%, respectively. In comparison, the BF-TT

CMP possessed an intermediate T_{d10} and char yield values of 414 $^\circ\text{C}$ and 65 wt%, respectively; and BIPE-TT CMP owned the lowest values and hence the down thermal stability up to 383 $^\circ\text{C}$ and 41 wt %, respectively (Fig. S10 and Table S1).

With a view to evaluate both the BET surface areas and microporous nature of the thiazolyl-linked CMPs, we applied depressed-temperature nitrogen adsorption–desorption isotherms. Prior to measurements, the studied samples were degassed under vacuum at 120 $^\circ\text{C}$ overnight. The typical isothermal curves obtained after analysis can be distinguished according to International Union of Pure and Applied Chemistry classification as isotherms with hysteresis of type H3 with apparent hysteresis loops confirming the wide range of microporosity and mesoporosity of the produced CMPs [Fig. 2(a–c)] [77]. The surface areas, pore size, and pore volumes deduced from the obtained isotherms are presented in Table S2. The conjugated polymer bearing the carbazole unit (BC-TT CMP) displayed the highest value of surface area up to 522 m^2/g , with considerable N_2 adsorption at a low relative pressure, whereas that of thiazolyl-linked polymers holding bifluorenylidene (BF-TT CMP) and diphenylethylene (BIPE-TT CMP) moieties showed good values of BET of 181 m^2/g and 159 m^2/g , respectively. The pore size distribution of the tested frameworks is showed in (Fig. 2a–c) insets, in which BC-TT CMP mainly possessed microscaled and mesoscaled pores centered at 1.06–1.79 and 1.82–3.65 nm, which is consistent with the predicted pore sizes (Scheme S7). Furthermore, BF-TT CMP had micropores and mesopores at around 0.11–3.96 nm, which is consistent with the predicted pore sizes (Scheme S8). The BIPE-TT CMP possessed microscaled and mesoscaled pores centered at 0.12–1.75 and 1.79–3.85 nm (Table S2), which is

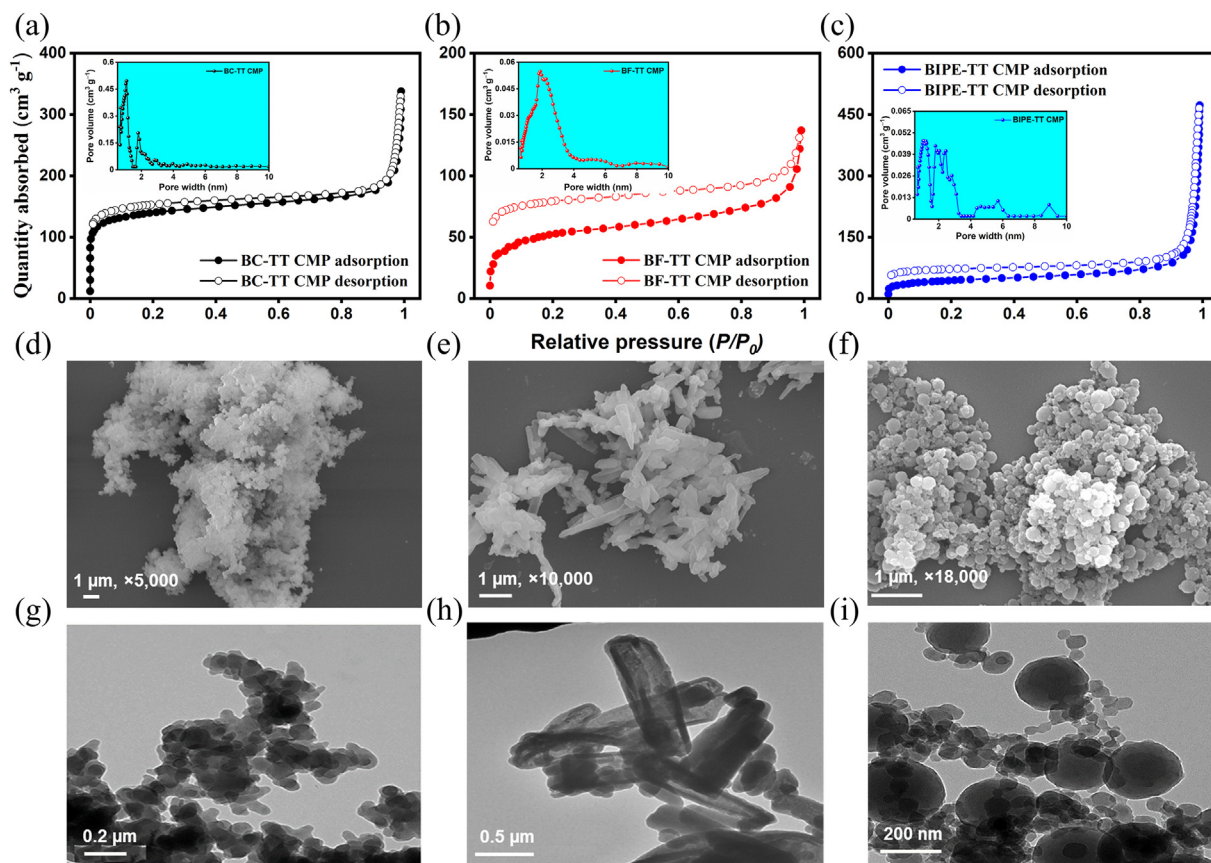


Fig. 2. Nitrogen sorption curves and the corresponding pore size distribution of (a) BC-TT, (b) BF-TT, and (c) BIPE-TT conjugated microporous polymers (CMPs); Scanning electron microscope images of (d) BC-TT, (e) BF-TT, and (f) BIPE-TT CMPs; The corresponding TEM images of (g) BC-TT, (h) BF-TT, and (i) BIPE-TT CMPs.

consistent with the predicted pore sizes (Scheme S9). These data suggested that the as-synthesized conjugated polymers owned a hierarchical pore structure, which could enhance the rate of mass transfer and facilitate the penetration of dye particles into thiazolyl-linked polymers, resulting in boosting their potential in adsorption application. The total pore volume was estimated from the N_2 uptake at high relative pressure ($P/P_0 = 0.99$). The pore volumes of BC-TT, BF-TT, and BIPE-TT CMPs were around 0.205–0.496, 0.054, and 0.041–0.047 cm^3/g , respectively (Table S2). The degree of π - π stacking between both of BF-TT and BIPE-TT CMPs sheets is higher than that of BC-TT CMP; consequently, their pore volumes and surface areas are lower than those of BC-TT CMP. The higher packing degree may have originated from the presence of the rigid double bond between the two fluorene units in the BF-TT polymer and the double bond between the two phenyl rings in the BIPE-TT polymer compared to the flexible single bond attached the nitrogen atoms of the two carbazole moieties in the BF-TT polymer [22].

Moreover, the porous characteristics of the CMPs were further confirmed by performing both scanning electron microscope (SEM) and transmission electron microscope (TEM) investigations. Starting with SEM images that showed the existence of stacked sheets for BC-TT CMP and rod-shaped aggregates for BF-TT CMP, in addition to spherical-shaped irregular particles for BIPE-TT CMP (Fig. 2d–f). As the TEM images depict, they have the same morphology mentioned previously for SEM, with nano-sheet structures for CMP bearing carbazole building block. Also, the bifluorenylidene-based polymer possessed micro-rod structures with a diameter ranging from 0.25 μm to 0.48 μm , and the polymers containing diphenylethylene moiety had spherical structures with diameter values ranging from 71 nm to 250 nm [Figs. 2g–i and S11].

3.2. Photophysical characterizations

The photophysical characterizations of the BC-TT, BF-TT and BIPE-TT CMPs were recorded by the solid-state UV-visible diffuse spectra. These polymers manifested broad visible light absorptions, with the maximum absorption wavelengths being 460 nm for BC-TT CMP, 272 nm for BF-TT CMP, and 276 nm for BIPE-TT CMP (Fig. 3a). This indicates that the as-prepared polymers have the great ability to harvest visible light for photocatalytic dye degradation. The optical bandgaps (E_g) were determined using Tauc plots being 2.27, 1.60, and 1.85 eV for BC-TT, BF-TT, and BIPE-TT CMPs, respectively, as shown in Fig. 3b. Accordingly, we can tune the E_g values by changing the donor units (BC, BF, BIPE). Comparison of these values with the most utilized ZnO photocatalyst E_g value (~ 3.45 eV) led to the fact that these polymers possess low optical band gaps and hence are more eligible for charge transfer interactions through the generated free radicals [78]. The highest

Table 1
Photophysical properties of thiazolyl-linked polymers.

Polymer	HOMO/LUMO (eV) ^{a,b}	Bandgap (eV) ^c
BC-TT CMP	−5.76/−3.49	2.27
BF-TT CMP	−5.81/−4.71	1.10
BIPE-TT CMP	−5.84/−3.99	1.85

CMP, conjugated microporous polymers; BC-TT, bicarbazol-thiazolyl polymer; BF-TT, bifluorenylidene-thiazolyl polymer; BIPE-TT, biphenylethene-thiazolyl polymer; HOMO, highest occupied molecular orbital; LUMO, lowest occupied molecular orbital.

^a HOMO calculated using photoelectron spectrometry.

^b LUMO = $E_{HOMO} - E_g$.

^c Bandgap calculated from Tauc plots.

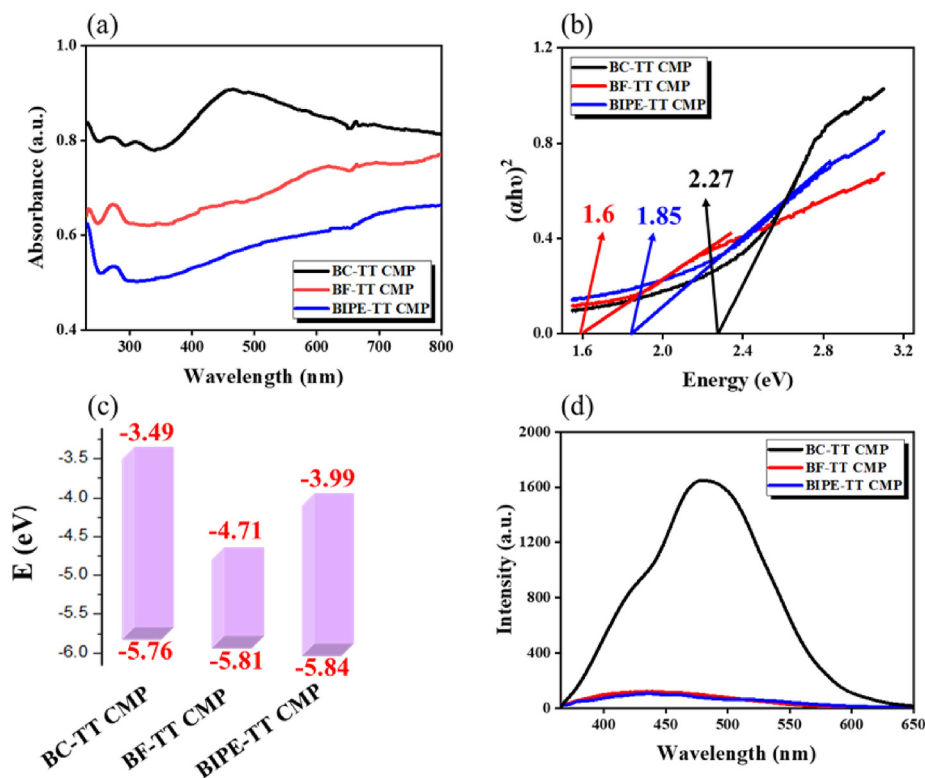


Fig. 3. (a) Ultraviolet (UV)-visible diffuse absorption spectra of the conjugated microporous polymers (CMPs); (b) Tauc plots derived from the UV-Visible spectra; (c) The electronic band structure of polymers; (d) Photoluminescence emission spectra of CMPs.

occupied molecular orbital (HOMO) energy levels for all CMPs were estimated using the photoelectron spectrometer. The lowest unoccupied molecular orbital (LUMO) energy levels were calculated using the following equation: $E_{LUMO} = E_{HOMO} + E_g$. As a result, the HOMO and LUMO values of BC-TT, BF-TT, and BIPE-TT CMPs were $-5.76/-3.49$ eV, $-5.81/-4.71$ eV, and $-5.84/-3.99$ eV, respectively (Figs. 3c, S12 and Table 1).

The photoinduced electron–hole pairs and their isolation and migration are among the fundamentals of photocatalytic process which can be measured using PL. As a law, the smaller the PL intensity, the better the charge separation. Consequently, the BIPE-TT CMP with the smallest PL intensity had the best efficiency of electron and hole separation. The PL intensities decreased in the following order: BIPE-TT CMP < BF-TT CMP < BC-TT CMP. The BC-TT CMP with the highest absorption intensity showed a red shift toward higher wavelengths (maximum wavelength up to 480 nm) comparable to BF-TT and BIPE-TT CMPs, which have maximum absorption bands at 425 and 435 nm, respectively (Fig. 3d). The PL data were extra-confirming the possibility of polymers' applications as photocatalysts in the visible range region (380–700 nm).

3.3. Dye uptake and recycling efficiency

Our synthesized thiazolyl-linked CMPs possessed some remarkable features, including high specific surface areas, large pores, narrow pore distribution, as well as the hydrophobic nature, which enable them to be applied as adsorbents for organic contaminations

in water. Also, they had a conjugated structure and high electron density located at nitrogen and sulfur atoms that facilitate the attraction forces of small organic adsorbates [27]. In addition, the presence of nitrogen atoms within the porous polymeric frameworks can enhance the dye uptake performance [76]. Therefore, the application of these CMPs in water treatment from soluble organic dyes as RhB and MB was investigated. After addition of a calculated amount of thiazolyl-linked CMPs (5 mg), UV-visible spectroscopy of the resultant solution was monitored at different time periods to follow the dye adsorption process. Taking RhB dye as an example, it was fully adsorbed in a short time by the BC-TT CMP, turning the solution color from deep violet red to nearly colorless, while the CMP became pink in color (Fig. 4d, insets). The dye uptake reached a plateau so quickly after a period of 30 min as observed from the intensity variation of the corresponding absorption peak at 554 nm (Fig. 4a). The same manner was noticed also with MB dye solutions onto BC-TT CMP, in which their absorption bands located at 664 nm were followed, which represented a considerable lowering of peak intensity with time evolution (Fig. 5a and d). The performance of RhB dye adsorption onto BC-TT polymer has reached about 98%, after 30 min from starting of experiment, whereas the efficiency of MB dye uptake reached 99.6% within 15 min. After 60 min, nearly a full dye removal was accomplished (99% for both RhB and MB), demonstrating our suggestion that the thiazolyl-linked CMPs under study have the potential capacity of eliminating organic dyes from polluted water. In comparison, within 1 h the percentage of RhB dye removal for BF-TT and BIPE-TT CMPs were 82% and 97%, respectively

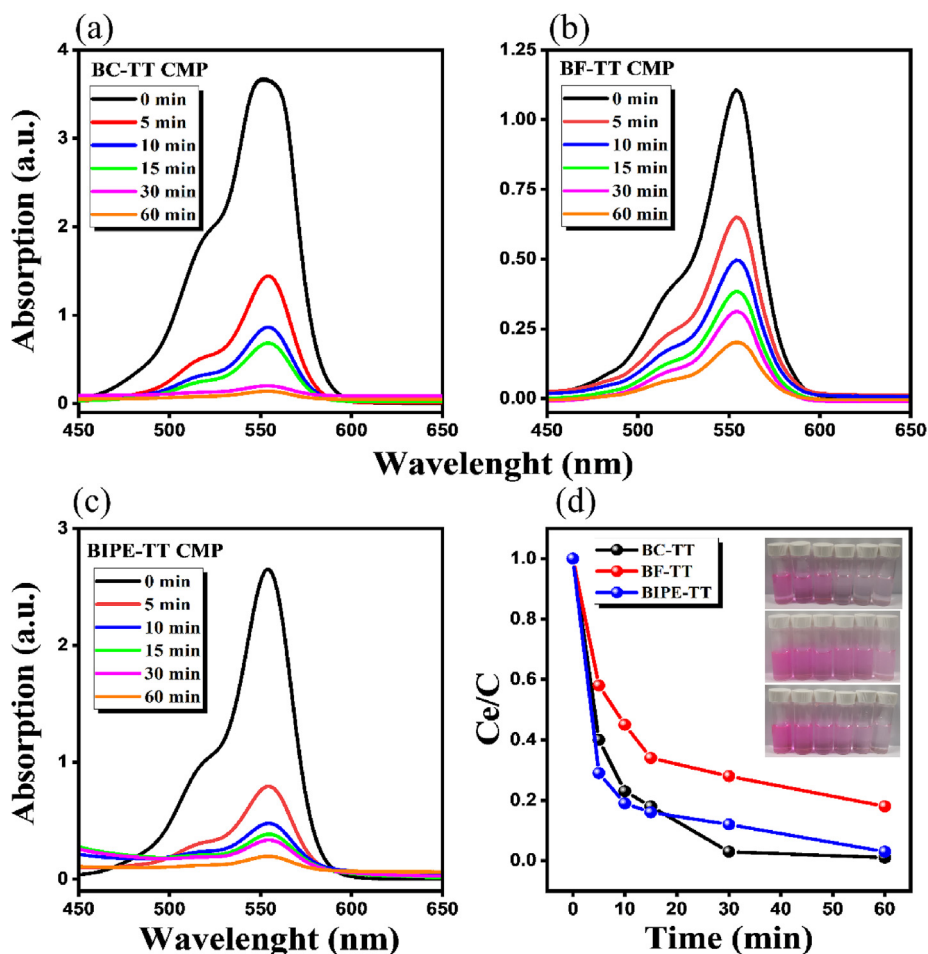


Fig. 4. (a–c) Ultraviolet-Visible spectroscopy of Rhodamine B (RhB) dye solution at various time intervals after the addition of the (a) BC-TT, (b) BF-TT, and (c) BIPE-TT conjugated microporous polymers (CMPs); (d) adsorption rates of RhB organic dye from an aqueous solution onto CMPs.

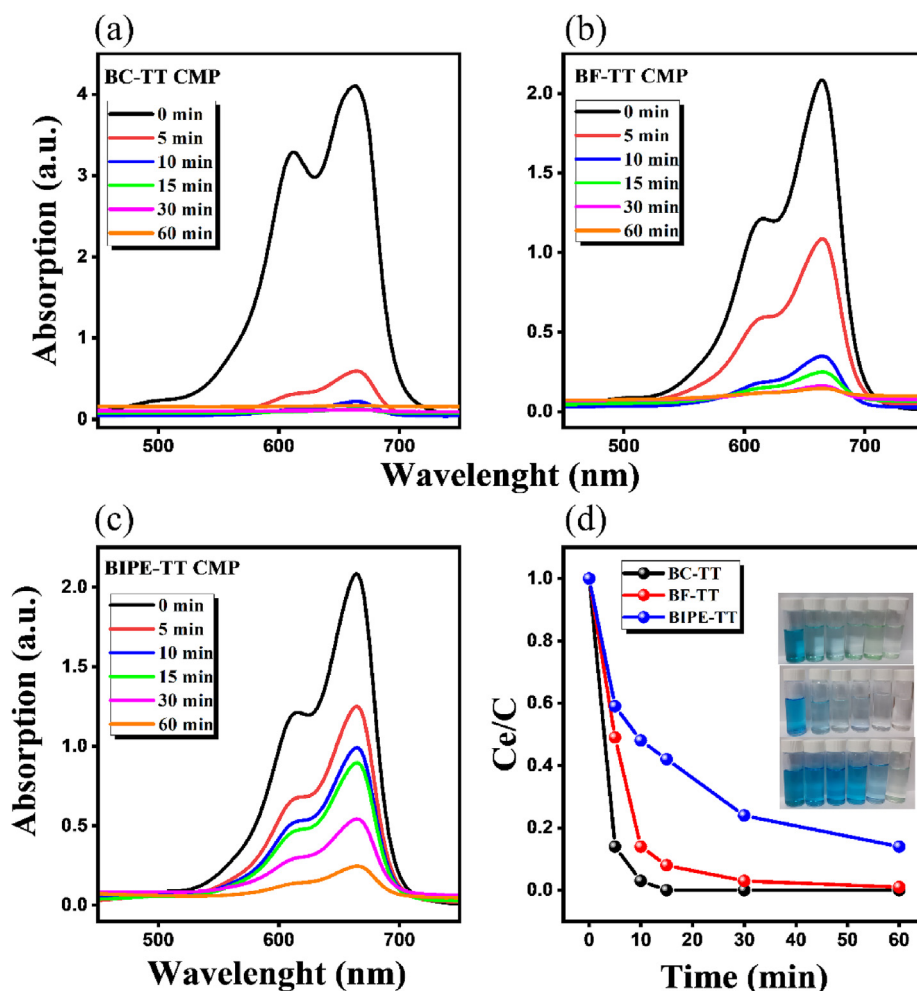


Fig. 5. (a–c) Ultraviolet-Visible spectroscopy of methylene blue (MB) dye solution at various time intervals after the addition of the (a) BC-TT, (b) BF-TT, and (c) BIPE-TT conjugated microporous polymers (CMPs); (d) adsorption rates of MB organic dye from an aqueous solution onto CMPs.

(Fig. 4b–d), whereas MB dye adsorption values were 99.2% and 85% for BF-TT and BIPE-TT CMPs, respectively (Fig. 5b–d). From the previous data, one can conclude that the BF-TT CMP has a higher efficiency than BIPE toward MB dye uptake (86% and 58% within 15 min for BF-TT and BIPE-TT CMPs, respectively). On the other hand, the BIPE-TT CMP has a greater activity than BF-TT CMP toward RhB dye adsorption (84% and 67% after 15 min for BIPE-TT and BF-TT CMPs, respectively). The experimental data confirm that many factors are responsible for the dye absorption efficacy such as BET surface area and N and S content of the polymers, in addition to the secondary interactions of the CMPs towards dye molecules. As a result, the BC-TT CMP, which possessed the highest surface area compared to the other CMPs (522 m²/g), recorded the best performance for dye adsorption. Also, the greater the number of nitrogen atoms, the more basicity of the resulting CMP surface, leading to improving dye interactions toward CMP surfaces through secondary chemical bonding. As a result, the top activity of dye uptake for the BC-TT CMP was also related to this reason. Furthermore, the adsorption effectiveness of the dye molecules was proved to be directly proportional to the degree of π – π stacking interaction of the adsorbent and adsorbate [79]. The BC-TT CMP was shown to have the strongest stacking between its carbazole units and the aromatic rings of both RhB, and MB molecules, which translated to the highest efficiency for water purification from these dye impurities. Accordingly, there are a higher number of dye molecules adsorbed on the surface of the BC-TT CMP, which can absorb and interact with a large

extent of the incident light, leading to the highest photocatalytic efficiency for dye degradation compared to the other synthesized CMPs. Similarly, both BF-TT and BIPE-TT CMPs had the same nitrogen and sulfur content and nearly identical pore volumes, but the former one showed a better performance due to the highest surface area and the presence of a considerable degree of stacking interactions in comparison to the latter CMP.

The produced adsorption data were fitted against the Langmuir model to investigate the adsorption manner of the used dyes on the surface of CMPs [80]. The maximum capacities for RhB dye adsorption on the surface of BC-TT CMP, BF-TT CMP, and BIPE-TT CMP were calculated to be 228.83, 97.47, and 170.65 mg/g, respectively (Figs. S13 and S14 and Table S3). To verify the universality of our thiazolyl-linked CMPs toward other organic dyes, the adsorption experiment of MB was also tested. Similarly, the calculated top values of adsorption capacities for MB were 232.02, 140.45, and 91.66 mg/g corresponding to BC-TT, BF-TT, and BIPE-TT polymers, respectively (Figs. S13 and S14 and Table S4). From these results, BC-TT CMP was considered the outstanding candidate for removing either RhB or MB from water (Table S5). In other words, the thiazolyl-linked CMP containing carbazole building unit displayed superior removal efficiency for water-soluble cationic organic dyes.

In our study, both RhB and MB organic dyes can be easily adsorbed on the surface of adsorbent polymers through Van der Waals force and acid–base interactions because our synthesized polymers are rich in nitrogen and sulfur atoms [81,82]. By

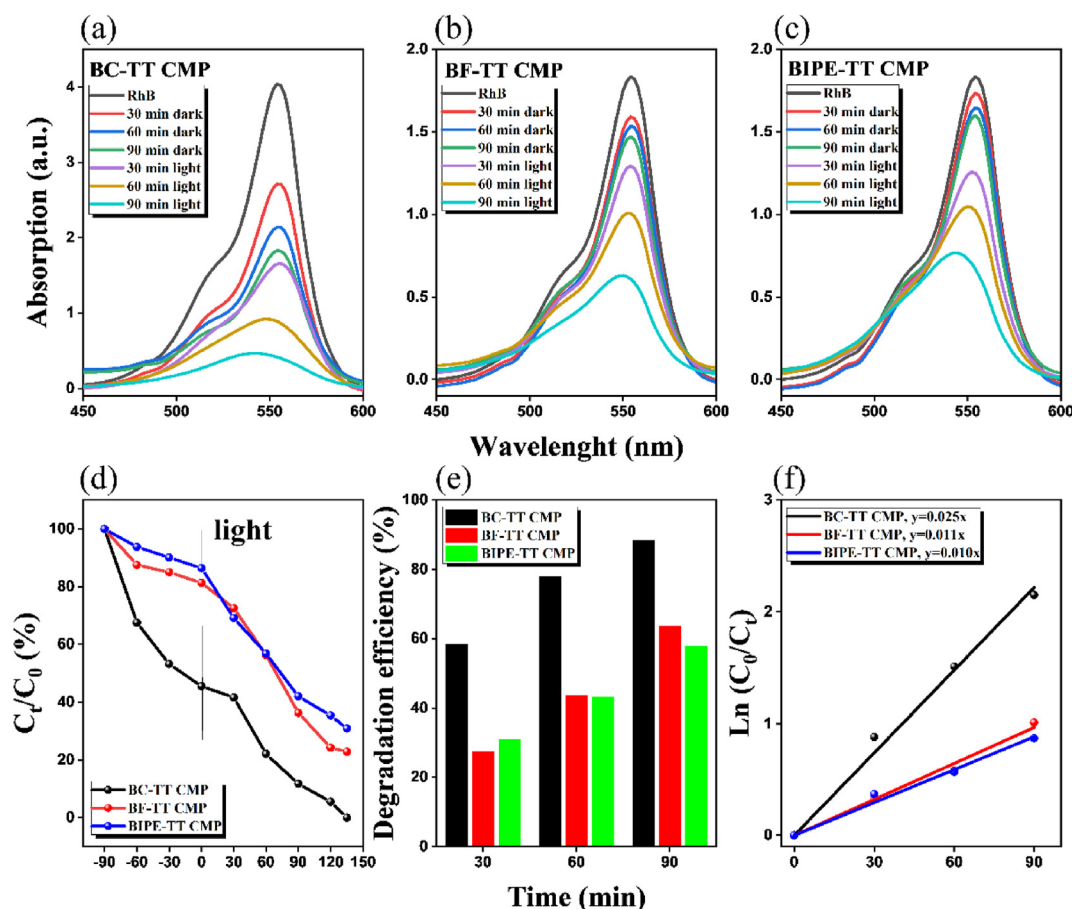


Fig. 6. (a–c) Ultraviolet-Visible spectroscopy for photocatalytic degradation of Rhodamine B (RhB) in water at different time intervals by (a) BC-TT, (b) BF-TT, and (c) BIPE-TT conjugated microporous polymers (CMPs); (d) photocatalytic performance of CMPs for RhB dye degradation under visible light irradiation at different time; (e) comparison of the efficiency of the CMPs for photocatalytic RhB degradation in aqueous solutions at various time; (f) Pseudo-first-order kinetic curves of photocatalytic degradation of RhB in aqueous solutions.

comparing the FTIR spectra of the thiazolyl-linked polymers before and after the dye uptake, it is clear to notice that the characteristic peaks of the resultant complex have slightly shifted after the dye adsorption. For example, the characteristic peak of C=C stretching vibrations of polymers has moved from 1,600, 1,600, and 1,598 cm^{-1} to 1,603, 1,603, and 1,601 cm^{-1} for BC-TT, BF-TT, and BIPE-TT CMPs, respectively, after RhB dye adsorption. Also, the C=O peak of RhB dye itself has shifted from 1,706 cm^{-1} to 1,735, 1,698, and 1,743 cm^{-1} after adsorption on the surfaces of BC-TT, BF-TT, and BIPE-TT CMPs, respectively (Figs. S15–S17). The same behavior was observed also after MB dye adsorption, in which the C=C peak of polymers was moved to 1,605, 1,603, and 1,608 cm^{-1} due to adsorption on the surfaces of BC-TT, BF-TT, and BIPE-TT CMPs, respectively (Figs. S18–S20).

3.4. Photocatalytic degradation

The adsorption and photodegradation behaviors of the CMPs toward RhB and MB upon irradiation with visible light were tested, and their data were displayed in Figs. S21 and S22. The small bandgap, high surface area, and good porosity of BC-TT CMP allowed the best photocatalytic efficiency, which was explored by degradation of dyes. Owing to different adsorption abilities, various concentrations of RhB and MB solutions were selected for BC-TT CMP (20 mg/L), BF-TT CMP (10 mg/L), and BIPE-TT CMP (10 mg/L). The photodegradation contribution was very clear, which can be distinguished from the normal physical adsorption in the absence

of light. BC-TT CMP displayed the highest efficacy of photocatalytic degradation of RhB and MB compared to all other thiazolyl-linked CMPs. Within 135 min of visible light irradiation (>450 nm) in the presence of BC-TT CMP, about 100% of RhB and 100% of MB were decomposed completely. This behavior was due to the highest surface area (522 m^2/g) and the suitable bandgap (2.27 eV) [83]. In comparison, BF-TT and BIPE-TT CMPs represented intermediate values of RhB dye degradation up to 80% and 75%, respectively after the same period, whereas MB dye degradation efficiencies were nearly the same with a value of 66% for both BF-TT and BIPE-TT CMPs.

Another study was established through the combination of conventional physisorption of RhB and MB organic dyes on the surface of CMPs within 90 min, followed by the catalytic photodegradation of these dyes within the next 90 min (Figs. 6a–d and 7a–d). The obtained results indicated the highest photocatalytic efficiency for the BC-TT CMP compared to both BF-TT and BIPE-TT CMPs. The performance of photodegradation of BC-TT CMP for RhB reaches 88.3% within a period of 90 min with a catalyst amount of 0.5 g/L, which is more than those of BF-TT CMP (63.7%) and BIPE-TT CMP (58%). The same behavior was also noticed for the photocatalytic MB degradation, in which BC-TT CMP was the best catalyst with a value of degradation of 96.2% in comparison to 74.7% and 50% for BF-TT and BIPE-TT CMPs, respectively, during 90 min with the same catalyst dose (Figs. 6e and 7e).

To establish photodegradation kinetics of RhB and MB organic dyes, the kinetic data of the photocatalytic reaction were fitted using the Langmuir–Hinshelwood kinetics model ($\ln(C_0/C_t) = kt$,

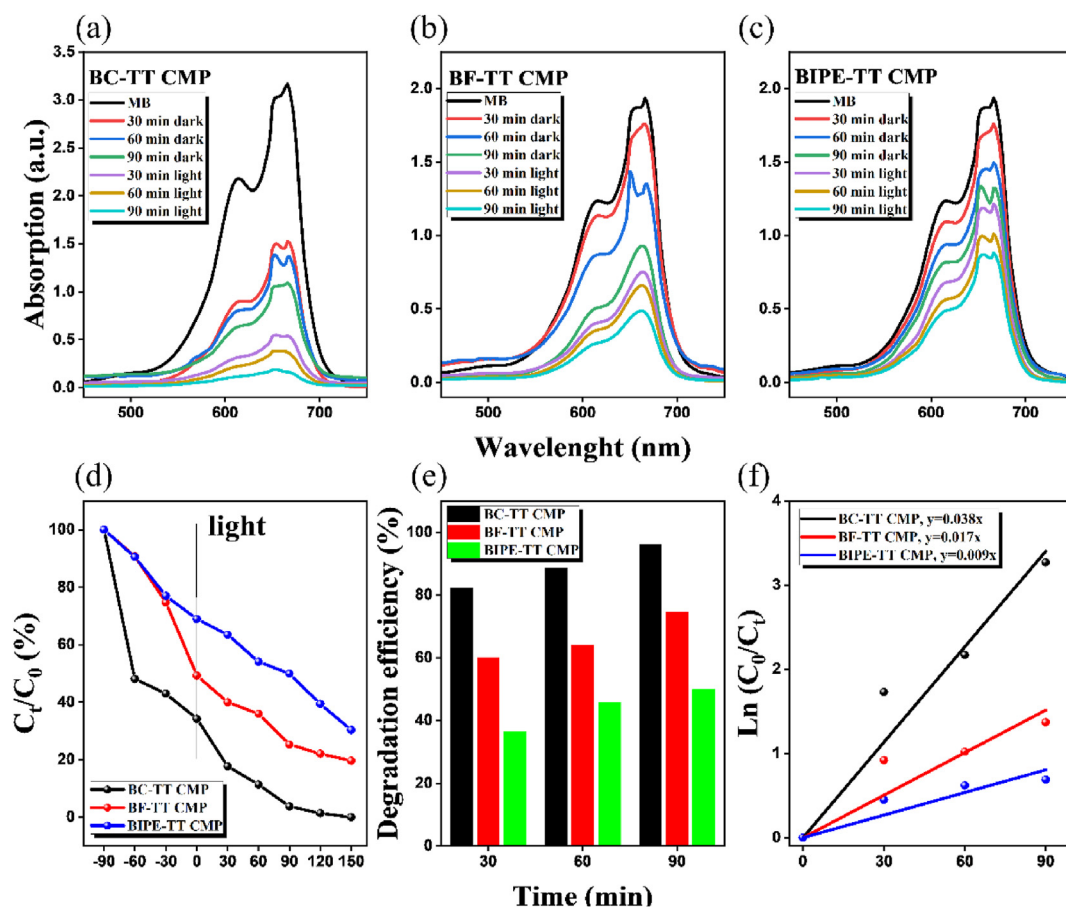


Fig. 7. (a–c) Ultraviolet-Visible spectroscopy of photocatalytic degradation of methylene blue (MB) in water at different time intervals by (a) BC-TT, (b) BF-TT, and (c) BIPE-TT conjugated microporous polymers (CMPs). (d) photocatalytic performance of CMPs for MB dye degradation under visible light irradiation at different time; (e) comparison of the efficiency of the CMPs for photocatalytic MB degradation in aqueous solutions at various time; (f) Pseudo-first-order kinetic curves of photocatalytic degradation of MB in aqueous solutions.

where C_0 and C_t are the concentrations of dye aqueous solution at $t = 0$ and t minutes of the photocatalytic reaction). Freundlich isotherms were also used for experimental fitting and rate calculations. The obtained curves indicated the pseudo-first-order reaction kinetics. BC-TT CMP demonstrated the highest catalytic efficiency in the photodegradation of RhB with a reaction rate constant of $2.5 \times 10^{-2} \text{ min}^{-1}$, which is 2.5-fold higher than those of BF-TT CMP ($1.1 \times 10^{-2} \text{ min}^{-1}$) and BIPE-TT CMP ($1.0 \times 10^{-2} \text{ min}^{-1}$). Similarly, the rate constant of BC-TT CMP for photocatalytic MB dye degradation was $3.5 \times 10^{-2} \text{ min}^{-1}$, which is also higher than those of BF-TT and BIPE-TT CMPs with values of $1.7 \times 10^{-2} \text{ min}^{-1}$ and $9 \times 10^{-3} \text{ min}^{-1}$, respectively. These results further confirm the superior photocatalytic performance of our thiazolyl-linked CMPs (Figs. 6f and 7f).

These efficiency values of dye degradation are competing those of many reported porous organic polymers. For example, Zhao et al. reported a facile fabrication of ultrathin two-dimensional covalent organic nanosheets (2D-CONs) via direct polymerization of monomers under ultrasonic treatment and a mild condition. The as-prepared ultrathin CONs showed significant heterogeneous photocatalytic efficacy for MB dye degradation. The triphenylbenzene CON (P-CON) possessed higher degradation efficiency with a reaction rate constant of $1.6 \times 10^{-2} \text{ min}^{-1}$, which was much higher than that of the triphenylbenzene COF (P-COF) with a reaction rate constant of $6.0 \times 10^{-3} \text{ min}^{-1}$ [84]. Also, our group has synthesized pyrrolo[3,2-*b*]pyrrolyl-based CMPs (Py-CMPs) through

a metal-free polycondensation of aryl aldehydes, aryl anilines, and a β -diketone. Py-CMP-2 showed strong photocatalytic RhB degradation, with a reaction rate constant of $3.4 \times 10^{-2} \text{ min}^{-1}$, which was greater than that of Py-CMP-1 with a value of $2.0 \times 10^{-3} \text{ min}^{-1}$ [64]. In addition, a range of phenyl- or thiophene-linked CTFs were synthesized by Liu et al. that exhibited an excellent photodegradation ability to acidic and basic dyes as well without addition of oxidant materials or pH adjustment. Particularly 3Ph-CTF was found to have the best values either for photocatalytic RhB dye degradation (with a reaction rate constant of $8.6 \times 10^{-2} \text{ min}^{-1}$) or MB dye degradation (with a reaction rate constant of $3.0 \times 10^{-2} \text{ min}^{-1}$) [85].

The kinetics rate for the as-synthesized CMPs were further confirmed by plotting $\ln(C_0/C_t)$ against time, which revealed the high kinetic rate of BC-TT CMP towards RhB and MB dyes' uptake compared to those of BF-TT and BIPE-TT CMPs (Fig. S23). The mechanism for photocatalytic degradation of organic dyes was investigated using trapping experiments. The common reactive species accepted for photocatalytic organic degradation are superoxide radical ($\cdot\text{O}_2^-$), hole (h^+), and hydroxyl radical ($\cdot\text{OH}$) [86,87]. *p*-Benzoquinone (BQ), methanol (MeOH), and isopropyl alcohol were applied as scavengers for $\cdot\text{O}_2^-$, h^+ , and $\cdot\text{OH}$, respectively, to test their function in the photocatalysis process. The obtained results demonstrated that the photodegradation efficiency of BC-TT CMP for RhB dye decreased upon addition of these trapping reagents (Figs. S24 and S25), confirming that $\cdot\text{O}_2^-$, h^+ , and $\cdot\text{OH}$

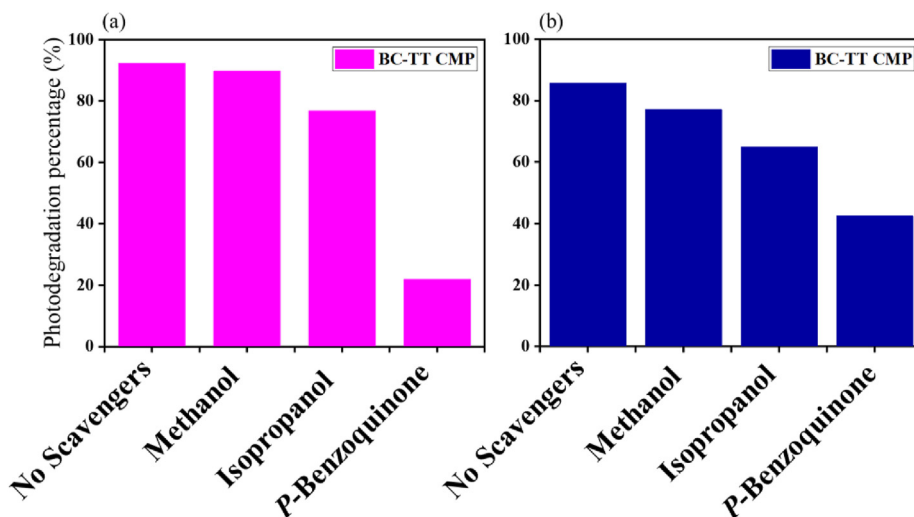


Fig. 8. Influence of different scavengers (Methanol, Isopropanol, and *p*-benzoquinone) onto photodegradation of (a) Rhodamine B organic dye, and (b) methylene blue organic dye over BC-TT conjugated microporous polymer under visible light irradiation for 60 min.

all participated in the photocatalytic degradation. The same behavior was noticed for the performance drop of BC-TT CMP toward MB dye degradation with all the reactive species involved in the process. Furthermore, a remarkable decrease of degradation activity was recorded when BQ was used as a scavenger, with a degradation efficiency of 21.95% for RhB dye and 42.5% for MB dye, leading to the fact that the crucial trapping reactive species is $\cdot\text{O}_2^-$ (Fig. 8). The recyclability of our thiazolyl-based CMPs was determined by measuring their FTIR spectra before and after RhB and MB photodegradation. The results demonstrated that there are no obvious changes either in the position or in the intensity of the absorption bands of the polymers, confirming their stability and reusability (Figs. S26–S28). Another experiment has been carried out to confirm their stability by immersing the synthesized CMPs in water and stirring for 48 h and then comparing their FTIR spectra before and after the experiment. From the obtained results, one can see that the position and intensity of all peaks are nearly the same without any changes that prove their potential application in dye uptake from water (Figs. S29–S31).

4. Conclusion

In conclusion, the three thiazolyl-linked CMPs have been easily synthesized via Suzuki polycondensation with dual application of both physisorption and photodegradation of organic dyes from water. The as-prepared CMPs possessed a considerable degree of porosity with BET surface area reaching $522 \text{ m}^2/\text{g}$, as well as high thermal stabilities as confirmed by the top value at $T_{d10} = 460 \text{ }^\circ\text{C}$, with the corresponding char yield value at 67%. BC-TT CMP was shown to have superior efficiency compared to the other CMPs in both physical adsorption and photodegradation of RhB and MB dyes because of its higher surface area, nitrogen content, and narrower bandgap as well. The highest adsorption efficiency was shown by BC-TT CMP with capacity values of 228.83 mg/g and 232.02 mg/g , for RhB and MB dyes removal, respectively. Upon measuring the photocatalytic degradation of dyes using these CMPs, the BC-TT CMP also had the highest value of catalytic efficiency of all, either for RhB dye (rate constant $2.5 \times 10^{-2} \text{ min}^{-1}$), or MB dye (rate constant $3.5 \times 10^{-2} \text{ min}^{-1}$). Our current work was from few examples in terms of removing soluble organic dyes from water by using both adsorption and photodegradation strategies, that demonstrate a new tactic ‘kill two birds with one stone’ for developing effective porous polymers for water treatment.

CRediT author statement

Ahmed F. Saber: Methodology, Conceptualization, Data curation, Investigation, Writing-Original draft preparation. **Chu-Chen Chueh:** Data curation, Investigation, Writing-Original draft preparation. **Mohamed Rashad:** Methodology, Data curation, Investigation, Writing-Original draft preparation. **Shiao-Wei Kuo:** Data curation, Investigation, Supervision. **Ahmed. F. M. EL-Mahdy:** Conceptualization, Data curation, Funding acquisition, Investigation, Project administration, Resources, Supervision, Validation, Visualization, Writing - review & editing.

Declaration of competing interest

The authors declare that they have no known competing financial interests or personal relationships that could have appeared to influence the work reported in this paper.

Data availability

Data will be made available on request.

Acknowledgments

This study was supported financially by the National Science and Technology Council, Taiwan, under contract NSTC 111-2221-E-110-003.

Appendix A. Supplementary data

Supplementary data to this article can be found online at <https://doi.org/10.1016/j.mtsust.2023.100429>.

References

- [1] H. Zhang, X. Lv, Y. Li, Y. Wang, J. Li, P25-graphene composite as a high performance photocatalyst, *ACS Nano* 4 (2010) 380–386.
- [2] A.A. Adeyemo, I.O. Adeoye, O.S. Bello, Metal organic frameworks as adsorbents for dye adsorption: overview, prospects and future challenges, *Toxicol. Environ. Chem.* 94 (2012) 1846–1863.
- [3] M.A. Shannon, P.W. Bohn, M. Elimelech, J.G. Georgiadis, B.J. Marinas, A.M. Mayes, Science and technology for water purification in the coming decades, *Nature* 452 (2008) 301–310.

- [4] N. Cheng, Q. Hu, Y. Guo, Y. Wang, L. Yu, Efficient and selective removal of dyes using imidazolium-based supramolecular gels, *ACS Appl. Mater. Interfaces* 7 (19) (2015) 10258–10265.
- [5] S.D. Richardson, S.Y. Kimura, Water analysis: emerging contaminants and current issues, *Anal. Chem.* 88 (1) (2015) 546–582.
- [6] J. Abdi, M. Vossoughi, N.M. Mahmoodi, I. Alemzadeh, Synthesis of metal-organic framework hybrid nanocomposites based on GO and CNT with high adsorption capacity for dye removal, *Chem. Eng. J.* 326 (2017) 1145–1158.
- [7] X. Pan, S. Cheng, T. Su, G. Zuo, W. Zhao, X. Qi, W. Wei, W. Dong, Fenton-like catalyst Fe_3O_4 @ polydopamine– MnO_2 for enhancing removal of methylene blue in wastewater, *Colloids Surf. B* 181 (2019) 226–233.
- [8] M. Hejtmancik, M. Ryan, J. Toft, R. Persing, P. Kurtz, R. Chhabra, Hematological effects in F344 rats and B6C3F1 mice during the 13-week gavage toxicity study of methylene blue trihydrate, *Toxicol. Sci.* 65 (1) (2002) 126–134.
- [9] J. Fu, Z. Chen, M. Wang, J. Zhang, J. Zhang, R. Han, Q. Xu, Adsorption of methylene blue by a high-efficiency adsorbent (polydopamine microspheres): kinetics, isotherm, thermodynamics and mechanism analysis, *Chem. Eng. J.* 259 (2015) 53–61.
- [10] M.S. Sajab, C.H. Chia, S. Zakaria, P.S. Khiew, Cationic and anionic modifications of oil palm empty fruit bunch fibers for the removal of dyes from aqueous solutions, *Bioresour. Technol.* 128 (2013) 571–577.
- [11] A. Benhouria, M.A. Islam, H. Zaghouane-Boudiaf, M. Boutahala, B.H. Hameed, Calcium alginate–bentonite-activated carbon composite beads as highly effective adsorbent for methylene blue, *Chem. Eng. J.* 270 (2015) 621–630.
- [12] R. Das, C.D. Vecitis, A. Schulze, B. Cao, A.F. Ismail, X. Lu, J. Chen, S. Ramakrishna, Recent advances in nanomaterials for water protection and monitoring, *Chem. Soc. Rev.* 46 (2017) 6946–7020.
- [13] S. Karaca, A. Gürses, M. Ağıkıldız, M. Ejder, Korucu, Adsorption of cationic dye from aqueous solutions by activated carbon, *Micropor. Mesopor. Mater.* 115 (3) (2008) 376–382.
- [14] S.K. Alpat, Ö. Özbayrak, Ş. Alpat, H. Akçay, The adsorption kinetics and removal of cationic dye, Toluidine Blue O, from aqueous solution with Turkish zeolite, *J. Hazard Mater.* 151 (1) (2008) 213–220.
- [15] S. Das, P. Heasman, B. Tan, S.L. Qiu, Porous organic materials: strategic design and structure–function correlation, *Chem. Rev.* 117 (2017) 1515–1563.
- [16] Y. Yuan, H.L. Huang, L. Chen, Y.L. Chen, N. N'-Bicarbazole: a versatile building block toward the construction of conjugated porous polymers for CO_2 capture and dyes adsorption, *Macromolecules* 50 (2017) 4993–5003.
- [17] T. Xu, Y. He, Y. Qin, C.X. Zhao, C.J. Peng, J. Hua, H.L. Liu, Facile preparation of porous organic copolymer based on triptycene and crown ether for efficient organic dye adsorption, *RSC Adv.* 8 (2018) 4963–4968.
- [18] X. Zhu, S.H. An, Y. Liu, L. Hu, H.L. Liu, C.C. Tian, S. Dai, X.J. Yang, H.L. Wang, C.W. Abney, S. Dai, Efficient removal of organic dye pollutants using covalent organic frameworks, *AlChE J.* 63 (2017) 3470–3478.
- [19] C. Wilson, M.J. Main, N.J. Cooper, M.E. Briggs, A.I. Cooper, D.J. Adams, Swellable functional hyper crosslinked polymer networks for the uptake of chemical warfare agents, *Polym. Chem.* 8 (2017) 1914–1922.
- [20] M.T. Ge, H.Z. Liu, A silsesquioxane-based thiophene-bridged hybrid nanoporous network as a highly efficient adsorbent for wastewater treatment, *J. Mater. Chem. A* 4 (2016) 16714–16722.
- [21] A.F.M. EL-Mahdy, J. Lüder, M.G. Kotp, S.W. Kuo, A Tröger's base-derived covalent organic polymer containing carbazole units as a high-performance supercapacitor, *Polymers* 13 (2021) 1385.
- [22] L.R. Ahmed, C.H. Chuang, J. Lüder, H.W. Yang, A.F.M. EL-Mahdy, Direct metal-free synthesis of uracil and pentaazaphenylene-functionalized porous organic polymers via quadruple Mannich cyclization and their nucleobase recognition activities, *Macromolecules* 55 (2022) 10197–10209.
- [23] P. Su, X. Zhang, Z. Xu, G. Zhang, C. Shen, Q. Meng, Amino-functionalized hypercrosslinked polymers for highly selective anionic dye removal and CO_2/N_2 separation, *New J. Chem.* 43 (2019) 17267–17274.
- [24] R. Dawson, A. Laybourn, R. Clowes, Y.Z. Khimyak, D.J. Adams, A.I. Cooper, Functionalized conjugated microporous polymers, *Macromolecules* 42 (2009) 8809–8816.
- [25] G. Xiong, B.B. Wang, L.X. You, B.Y. Ren, Y.K. He, F. Ding, I. Dragutan, V. Dragutan, Y.G. Sun, Hypervalent silicon-based, anionic porous organic polymers with solid microsphere or hollow nanotube morphologies and exceptional capacity for selective adsorption of cationic dyes, *J. Mater. Chem. A* 7 (2019) 393–404.
- [26] Y. Li, C.X. Yang, H.L. Qian, X. Zhao, X.P. Yan, Carboxyl-functionalized covalent organic frameworks for the adsorption and removal of triphenylmethane dyes, *ACS Appl. Nano Mater.* 2 (2019) 7290–7298.
- [27] T. Ben, H. Ren, S. Ma, D. Cao, J. Lan, X. Jing, W. Wang, J. Xu, F. Deng, J.M. Simmons, S. Qiu, G. Zhu, Targeted synthesis of a porous aromatic framework with high stability and exceptionally high surface area, *Angew. Chem., Int. Ed.* 48 (2009) 9457–9460.
- [28] T.-L. Lee, A.M. Elewa, M.G. Kotp, H.-H. Chou, A.F.M. EL-Mahdy, Carbazole-and thiophene-containing conjugated microporous polymers with different planarity for enhanced photocatalytic hydrogen evolution, *Chem. Commun.* 57 (2021) 11968–11971.
- [29] Y. Xu, S. Jin, H. Xu, A. Nagai, D. Jiang, Conjugated microporous polymers: design, synthesis and application, *Chem. Soc. Rev.* 42 (2013) 8012–8031.
- [30] M.G. Kotp, N.L. Torad, J. Lüder, A.A.M. El-Amir, W. Chaikittisilp, Y. Yamauchi, A.F.M. EL-Mahdy, A phenazine-conjugated microporous polymer-based quartz crystal microbalance for sensitive detection of formaldehyde vapors at room temperature: an experiment and density functional theory study, *J. Mater. Chem. A* 11 (2023) 764–774.
- [31] L. Chen, Y. Honsho, S. Seki, D. Jiang, Light-harvesting conjugated microporous polymers: rapid and highly efficient flow of light energy with a porous polypyrrole framework as antenna, *J. Am. Chem. Soc.* 132 (2010) 6742–6748.
- [32] L.R. Ahmed, L. Gilmanova, C.T. Pan, S. Kaskel, A.F.M. EL-Mahdy, Hollow spherical covalent organic frameworks from nonplanar or planar monomers for the fluorescence detection of telomere DNA: role of the 2-(2-azidoethoxy) ethoxy group, *ACS Appl. Polym. Mater.* 4 (2022) 9132–9143.
- [33] H.M. El-Kaderi, J.R. Hunt, J.L. Mendoza-Cortes, A.P. Cote, R.E. Taylor, M. O'Keeffe, O.M. Yaghi, Designed synthesis of 3D covalent organic frameworks, *Science* 316 (2007) 268–272.
- [34] A.M. Elewa, A.F.M. EL-Mahdy, A.E. Hassan, Z. Wen, J. Jayakumar, T.L. Lee, L.Y. Ting, I.M.A. Mekhemer, T.F. Huang, M.H. Elsayed, C.L. Chang, W.C. Lin, H.H. Chou, Solvent polarity tuning to enhance the crystallinity of 2D-covalent organic frameworks for visible-light-driven hydrogen generation, *J. Mater. Chem. A* 10 (2022) 12378–12390.
- [35] S.K. Kundu, A. Bhaumik, Novel nitrogen and sulfur rich hyper-cross-linked microporous poly-triazine-thiophene copolymer for superior CO_2 capture, *ACS Sustain. Chem. Eng.* 4 (2016) 3697–3703.
- [36] S. Mondal, S. Chatterjee, S. Mondal, A. Bhaumik, Thioether-functionalized covalent triazine nanospheres: a robust adsorbent for mercury removal, *ACS Sustain. Chem. Eng.* 7 (2019) 7353–7361.
- [37] S. Ruidas, A. Chowdhury, A. Ghosh, S. Mondal, A.D.D. Wanonke, M. Addicoat, A.K. Das, A. Modak, A. Bhaumik, Covalent organic framework as a metal-free photocatalyst for dye degradation and radioactive iodine adsorption, *Langmuir* 39 (2023) 4071–4081.
- [38] S. Xu, G. Wang, B.P. Biswal, M. Addicoat, S. Paasch, W. Sheng, X. Zhuang, E. Brunner, T. Heine, R. Berger, X. Feng, A nitrogen-rich 2D sp^2 -carbon-linked conjugated polymer framework as a high-performance cathode for lithium-ion batteries, *Angew. Chem. Int. Ed.* 58 (2018) 849–853.
- [39] C.F. Yao, K.L. Wang, H.K. Huang, Y.J. Lin, Y.Y. Lee, C.W. Yu, C.J. Tsai, M. Horie, Cyclopentadithiophene–terephthalic acid copolymers: synthesis via direct arylation and saponification and applications in Si-based lithium-ion batteries, *Macromolecules* 50 (2017) 6924–6934.
- [40] H. Wang, Z. Cheng, Y. Liao, J. Li, J. Weber, A. Thomas, C.F.J. Faul, Conjugated microporous polycarbazole networks as precursors for nitrogen-enriched microporous carbons for CO_2 storage and electrochemical capacitors, *Chem. Mater.* 29 (2017) 4885–4893.
- [41] X. Yan, M. Xiong, J.T. Li, S. Zhang, Z. Ahmad, Y. Lu, Z.Y. Wang, Z.F. Yao, J.Y. Wang, X. Gu, T. Lei, Pyrazine-flanked diketopyrrolopyrrole (DPP): a new polymer building block for high-performance n-type organic thermoelectrics, *J. Am. Chem. Soc.* 141 (2019) 20215–20221.
- [42] R. Sun, S. Feng, B. Zhou, Z. Chen, D. Wang, H. Liu, Flexible cyclosiloxane-linked fluorescent porous polymers for multifunctional chemical sensors, *ACS Macro Lett.* 9 (2020) 43–48.
- [43] L.R. Ahmed, A.F.M. EL-Mahdy, C.-T. Pan, S.W. Kuo, A water-soluble copper-immobilized covalent organic framework functioning as an “OFF–ON” fluorescent sensor for amino acids, *Mater. Adv.* 2 (2021) 4617–4629.
- [44] V. Lakshmi, C.H. Liu, M.R. Rao, Y. Chen, Y. Fang, A. Dadvand, E. Hamzehpoor, Y. Sakai-Ohtsuka, R.S. Stein, D.F. Perepichka, A two-dimensional poly(azatriangulene) covalent organic framework with semiconducting and paramagnetic states, *J. Am. Chem. Soc.* 142 (2020) 2155–2160.
- [45] S.H. Kang, A. Jeong, H.R. Lee, J.H. Oh, C. Yang, Bioderived and eco-friendly solvent-processed high-mobility ambipolar plastic transistors through controlled irregularity of the polymer backbone, *Chem. Mater.* 31 (2019) 3831–3839.
- [46] Y. Du, H. Yao, L. Galuska, F. Ge, X. Wang, H. Lu, G. Zhang, X. Gu, L. Qiu, Side-chain engineering to optimize the charge transport properties of isoindigo-based random terpolymers for high-performance organic field-effect transistors, *Macromolecules* 52 (2019) 4765–4775.
- [47] F. Chen, Y. Jiang, Y. Sui, J. Zhang, H. Tian, Y. Han, Y. Deng, W. Hu, Y. Geng, Donor–acceptor conjugated polymers based on bisisoindigo: energy level modulation toward unipolar n-type semiconductors, *Macromolecules* 51 (2018) 8652–8661.
- [48] T.M. Swager, 50th anniversary perspective: conducting/semiconducting conjugated polymers. A personal perspective on the past and the future, *Macromolecules* 50 (2017) 4867–4886.
- [49] A.F. Saber, S.U. Sharma, J.T. Lee, A.F.M. EL-Mahdy, S.W. Kuo, Carbazole-conjugated microporous polymers from Suzuki–Miyaura coupling for supercapacitors, *Polymer* 254 (2022) 125070–125076.
- [50] K.Y. Lin, A.F.M. EL-Mahdy, Covalent triazine frameworks based on triphenylpyridine building block for high-performance supercapacitor and selective CO_2 capture, *Mater. Chem. Phys.* 281 (2022), 125850.
- [51] T.L. Yang, J.Y. Chen, S.W. Kuo, C.T. Lo, A.F.M. EL-Mahdy, Hydroxyl-functionalized covalent organic frameworks as high-performance supercapacitors, *Polymers* 14 (2022) 3428.
- [52] B. Alameddine, S. Shetty, N. Baig, S. Al-Mousawi, Star-shaped tetra- and octa-arylamine triptycene-based dendrimers: modular building blocks for blue emission materials, *Mater. Today Chem.* 14 (2019) 100190–100197.
- [53] A. Leventis, J. Royakkers, A.G. Rapis, N. Goodeal, M.K. Corpinot, J.M. Frost, D.K. Bučar, M.O. Blunt, F. Cacialli, H. Bronstein, Highly luminescent encapsulated narrow bandgap polymers based on diketopyrrolopyrrole, *J. Am. Chem. Soc.* 140 (2018) 1622–1626.

- [54] A. Ichige, H. Saito, J. Kuwabara, T. Yasuda, J.C. Choi, T. Kanbara, Facile synthesis of thienopyrroledione-based π -conjugated polymers via direct arylation polycondensation under aerobic conditions, *Macromolecules* 51 (2018) 6782–6788.
- [55] M.J. Sung, S. Yoon, S.K. Kwon, Y.H. Kim, D.S. Chung, Synthesis of phenanthro [1,10,9,8-cdefg]carbazole-based conjugated polymers for green-selective organic photodiodes, *ACS Appl. Mater. Interfaces* 8 (2016) 31172–31178.
- [56] Y. Liao, Z. Cheng, W. Zuo, A. Thomas, C.F.J. Faul, Nitrogen-rich conjugated microporous polymers: facile synthesis, efficient gas storage, and heterogeneous catalysis, *ACS Appl. Mater. Interfaces* 9 (2017) 38390–38400.
- [57] S. Roy, A. Bandyopadhyay, M. Das, P.P. Ray, S.K. Pati, T.K. Maji, Redox-active and semi-conducting donor–acceptor conjugated microporous polymers as metal-free ORR catalysts, *J. Mater. Chem. A* 6 (2018) 5587–5591.
- [58] H. Wei, F. Wang, X. Qian, S. Li, Z. Hu, H. Sun, Z. Zhu, W. Liang, C. Ma, A. Li, Superhydrophobic fluorine-rich conjugated microporous polymers monolithic nanofoam with excellent heat insulation property, *Chem. Eng. J.* 351 (2018) 856–866.
- [59] Y. Xu, N. Mao, C. Zhang, X. Wang, J. Zeng, Y. Chen, F. Wang, J.X. Jiang, Rational design of donor– π -acceptor conjugated microporous polymers for photocatalytic hydrogen production, *Appl. Catal. Environ.* 228 (2018) 1–9.
- [60] A.F. Saber, A.M. Elewa, H.H. Chou, A.F.M. EL-Mahdy, Donor-acceptor carbazole-based conjugated microporous polymers as photocatalysts for visible-light-driven H_2 and O_2 evolution from water splitting, *Appl. Catal. B Environ.* 316 (2022) 121624–121633.
- [61] F. Wang, F. Ren, D. Ma, P. Mu, H. Wei, C. Xiao, Z. Zhu, H. Sun, W. Liang, J. Chen, L. Chen, A. Li, Particle and nanofiber shaped conjugated microporous polymers bearing hydantoin-substitution with high antibacterial activity for water cleanliness, *J. Mater. Chem. A* 6 (2018) 266–274.
- [62] A.F.M. EL-Mahdy, H.A.E. Omer, Z.A. AlOthman, H. Lee, Design and synthesis of metal-free ethene-based covalent organic framework photocatalysts for efficient, selective, and long-term stable CO_2 , *J. Colloid Interface Sci.* 633 (2023) 775–785.
- [63] A.F. Saber, A.M. Elewa, H.H. Chou, A.F.M. EL-Mahdy, Donor to acceptor charge transfer in carbazole-based conjugated microporous polymers for enhanced visible-light-driven photocatalytic water splitting, *ChemCatChem* 15 (2023), e202201287.
- [64] J.H. Wang, C.L. Chang, Z.W. Zhang, A.F.M. EL-Mahdy, Facile metal-free synthesis of pyrrolo [3, 2-b] pyrrolyl-based conjugated microporous polymers for high-performance photocatalytic degradation of organic pollutants, *Poly. Chem.* 13 (2022) 5300–5308.
- [65] A.N. Woodward, J.M. Kolesar, S.R. Hall, N.A. Saleh, D.S. Jones, M.G. Walter, Thiazolothiazole fluorophores exhibiting strong fluorescence and viologen-like reversible electrochromism, *J. Am. Chem. Soc.* 139 (25) (2017) 8467–8473.
- [66] M. Moral, A. Garzón, J. Canales-Vázquez, J.C. Sancho-García, Optoelectronic and semiconducting properties of conjugated polymers composed of thiazolo [5,4-d]thiazole and arene imides linked by ethynylene bridges, *J. Phys. Chem. C* 120 (2016) 24583–24596.
- [67] M. Samal, S. Valligatla, N.A. Saad, M.V. Rao, D.N. Rao, R. Sahu, B.P. Biswal, A thiazolo[5,4-d]thiazole-bridged porphyrin organic framework as a promising nonlinear optical material, *Chem. Commun.* 55 (74) (2019) 11025–11028.
- [68] G. Reginato, A. Mordini, L. Zani, M. Calamante, A. Dessì, Photoactive compounds based on the thiazolo[5,4-d]thiazole core and their application in organic and hybrid photovoltaics, *Eur. J. Org. Chem.* 2016 (2) (2016) 233–251.
- [69] A. Dessì, M. Calamante, A. Mordini, M. Peruzzini, A. Sinicropi, R. Basosi, F.F. de Biani, M. Taddei, D. Colonna, A. di Carlo, G. Reginato, L. Zani, Thiazolo[5,4-d]thiazole-based organic sensitizers with strong visible light absorption for transparent, efficient and stable dye-sensitized solar cells, *RSC Adv.* 5 (2015) 32657–32668.
- [70] D. Bevk, L. Marin, L. Lutsen, D. Vanderzande, W. Maes, Thiazolo[5,4-d]thiazoles promising building blocks in the synthesis of semiconductors for plastic electronics, *RSC Adv.* 3 (2013) 11418–11431.
- [71] I. Osaka, G. Sauvé, R. Zhang, T. Kowalewski, R.D. McCullough, Novel thiophene-thiazolothiazole copolymers for organic field-effect transistors, *Adv. Mater.* 19 (2007) 4160–4165.
- [72] X. Zhu, C. Tian, T. Jin, J. Wang, S.M. Mahurin, W. Mei, Y. Xiong, J. Hu, X. Feng, H. Liu, Thiazolothiazole-linked porous organic polymers, *Chem. Commun.* 50 (2014) 15055–15058.
- [73] A.V. Akkuratov, S.L. Nikitenko, A.S. Kozlov, P.M. Kuznetsov, I.V. Martynov, N.V. Tukachev, A. Zhugayevych, I. Visoly-Fisher, E.A. Katz, P.A. Troshina, Design of novel thiazolo-thiazole containing conjugated polymers for organic solar cells and modules, *Sol. Energy* 198 (2020) 605–611.
- [74] C.L. Chang, A.M. Elewa, J.H. Wang, H.H. Chou, A.F.M. EL-Mahdy, Donor–acceptor conjugated microporous polymers based on Thiazolo [5, 4-d] thiazole building block for high-performance visible-light-induced H_2 production, *Micropor. Mesopor. Mater.* 345 (2022), 112258.
- [75] D. Chen, W. Chen, G. Xing, T. Zhang, L. Chen, An upgraded “two-in-one” strategy toward highly crystalline covalent organic frameworks, *Chem. Eur. J.* 26 (2020) 8377–8381.
- [76] A.F.M. EL-Mahdy, M.B. Zakaria, H.X. Wang, T. Chen, Y. Yamauchi, S.W. Kuo, Heteroporous bifluorenylidene-based covalent organic frameworks displaying exceptional dye adsorption behavior and high energy storage, *J. Mater. Chem. A* 8 (2020) 25148–25155.
- [77] S.S. Chang, B. Clair, J. Ruelle, J. Beauchene, F.D. Renzo, F. Quignard, G.J. Zhao, H. Yamamoto, J. Gri, Mesoporosity as a new parameter for understanding tension stress generation in trees, *J. Exp. Bot.* 60 (2009) 3023–3030.
- [78] K. Preet, G. Gupta, M. Kotal, S.K. Kansal, D.B. Salunke, H.K. Sharma, S.C. Sahoo, P.V.D. Voort, S. Roy, Mechanochemical synthesis of a new triptycene-based imine-linked covalent organic polymer for degradation of organic dye, *Cryst. Growth Des.* 19 (2019) 2525–2530.
- [79] S.Y. Ding, J. Gao, Q. Wang, Y. Zhang, W.G. Song, C.Y. Su, W. Wang, Construction of covalent organic framework for catalysis: Pd/COF-LZU1 in Suzuki–Miyaura coupling reaction, *J. Am. Chem. Soc.* 133 (2011) 19816–19822.
- [80] I. Langmuir, The adsorption of gases on plane surfaces of glass mica and platinum, *J. Am. Chem. Soc.* 40 (1918) 1361–1403.
- [81] L. Liu, Z.Y. Gao, X.P. Su, X. Chen, L. Jiang, J.M. Yao, Adsorption removal of dyes from single and binary solutions using a cellulose-based bioadsorbent, *ACS Sustainable Chem. Eng.* 3 (2015) 432–442.
- [82] S. Ghorai, A. Sarkar, M. Raoufi, A.B. Panda, H. Schonherr, S. Pal, Enhanced removal of methylene blue and methyl violet dyes from aqueous solution using a nanocomposite of hydrolyzed polyacrylamide grafted xanthan gum and incorporated nanosilica, *ACS Appl. Mater. Interfaces* 6 (2014) 4766–4777.
- [83] B.C. Ma, S. Ghasimi, K. Landfester, F. Vilela, K.A.I. Zhang, Conjugated microporous polymer nanoparticles with enhanced dispersibility and water compatibility for photocatalytic applications, *J. Mater. Chem. A* 3 (2015) 16064–16071.
- [84] S.X. Gan, C. Jia, Q.Y. Qi, X. Zhao, A facile and scale-up synthetic method for covalent organic nanosheets: ultrasonic polycondensation and photocatalytic degradation of organic pollutants, *Chem. Sci.* 13 (2022) 1009–1015.
- [85] Y. Du, H. Ai, Y. Liu, H. Liu, A novel covalent triazine-based frameworks as photocatalysts for the degradation of dyes under visible light irradiation, *Sustain. Energy Fuels* 7 (2023) 1747–1754.
- [86] B. Wang, Z. Xie, Y. Li, Z. Yang, L. Chen, Dual-functional conjugated nanoporous polymers for efficient organic pollutants treatment in water: a synergistic strategy of adsorption and photocatalysis, *Macromolecules* 51 (2018) 3443–3449.
- [87] Y. Yang, H. Niu, L. Xu, H. Zhang, Y. Cai, Triazine functionalized fully conjugated covalent organic framework for efficient photocatalysis, *Appl. Catal. B Environ.* 269 (2020), 118799.